

Supplementary Information:

Structures and terahertz dynamics of imidazolium-based ionic liquid on a gold electrode studied using surface-enhanced Raman scattering

Ryo Ueno,¹ Kenta Motobayashi,¹ and Katsuyoshi Ikeda^{*,1}

¹Program of Applied Physics, Graduate School of Engineering, Nagoya Institute of Technology, Gokiso-cho, Showa, Nagoya 466-8555, Japan

*e-mail: kikeda@nitech.ac.jp

1. Normal Raman and SERS spectra in density of states (DOS) formats^{31,32}

To describe Raman scattering process, the absolute wavenumber ($\tilde{\nu} > 0$ in cm^{-1}) and the relative wavenumber ($\tilde{\nu}^{\Delta}$ in cm^{-1}) are used in the following equations by considering the connection to traditional wavenumber plotting in Raman spectrum. A power spectrum for normal Raman scattering, $I_{\text{RS}}(\tilde{\nu}^{\Delta})$, is connected with the imaginary part of the dynamic susceptibility, $\chi_{\text{RS}}''(\tilde{\nu})$, by the following expressions:

$$I_{\text{RS}}(\tilde{\nu}_{\text{as}}^{\Delta}) = K \cdot (\tilde{\nu}_0 + \tilde{\nu})^3 \cdot [n(\tilde{\nu})] \cdot \chi_{\text{RS}}''(\tilde{\nu}) \quad (1)$$

for anti-Stokes branch and

$$I_{\text{RS}}(\tilde{\nu}_{\text{s}}^{\Delta}) = K \cdot (\tilde{\nu}_0 - \tilde{\nu})^3 \cdot [n(\tilde{\nu}) + 1] \cdot \chi_{\text{RS}}''(\tilde{\nu}) \quad (2)$$

for Stokes branch of the spectrum. Here, $\tilde{\nu}_0$ is the photon energy for the incident laser ($\tilde{\nu}_0 = 1/632.8 \text{ nm} = 15802.8 \text{ cm}^{-1}$ (1.96 eV) in the present case). $\tilde{\nu}$ is the energy exchanged between photon and Raman scatterer; photon is scattered by a molecular vibration in the case of vibrational Raman scattering (vRS) or by a free electron of metal in the case of electronic Raman scattering (eRS). $\tilde{\nu}_{\text{as}}^{\Delta}$ and $\tilde{\nu}_{\text{s}}^{\Delta}$ are the Raman shifts relative to $\tilde{\nu}_i$ in the anti-Stokes and Stokes branches, *i.e.*, $\tilde{\nu}_{\text{as}}^{\Delta} = -\tilde{\nu}$ and $\tilde{\nu}_{\text{s}}^{\Delta} = \tilde{\nu}$. K is an instrument function. $[n(\tilde{\nu})]$ and $[n(\tilde{\nu}) + 1]$ correspond to thermal factors for the anti-Stokes and Stokes processes, respectively, and $n(\tilde{\nu})$ is the Bose-Einstein (BE) distribution described as $n(\tilde{\nu}) = [\exp(hc\tilde{\nu}/k_{\text{B}}T) - 1]^{-1}$, where h , c and k_{B} are Planck's constant, the velocity of light and the

Boltzmann constant, respectively. The BE thermal factor describes the thermal occupation of the photon states in Raman scattering. In short, Eqs (1) and (2) mean that Raman scattering intensity is proportional to the product of the photon states and the matter states ($\chi_{RS}''(\tilde{\nu})$). The matter states for vRS are given by vibrational density of states (VDOS) of molecule and those for eRS are given by electron-hole joint density of states (JDOS) of metal substrate. Therefore, a measured Raman spectrum can be converted to the DOS format by reducing the frequency factor and the BE thermal factor.

There is a broad consensus that SERS is a vibrational spectroscopy; molecular vibration signals, *i.e.*, vRS signals, are plasmonically enhanced on a metal surface. However, eRS signals from metal substrate can also gain intensity from surface plasmon polaritons, which causes a background continuum in a SERS spectrum. Here, SERS effect for vRS and eRS are denoted as vSERS and eSERS, respectively. To describe vSERS, Eqs. (1) and (2) can be modified like:

$$I_{\text{vSERS}}(\tilde{\nu}_{\text{as}}^{\Delta}) = K \cdot (\tilde{\nu}_0 + \tilde{\nu})^3 \cdot [n(\tilde{\nu}) + 1] \cdot \left[\frac{E_{\text{loc}}^{\text{d}}(\tilde{\nu}_0 + \tilde{\nu})}{E_0(\tilde{\nu}_0 + \tilde{\nu})} \right]^2 \cdot \left[\frac{E_{\text{loc}}^{\text{d}}(\tilde{\nu}_0)}{E_0(\tilde{\nu}_0)} \right]^2 \cdot g^{\text{d}} \cdot \chi_{\text{vRS}}''(\tilde{\nu}) \quad (3)$$

for anti-Stokes branch and

$$I_{\text{vSERS}}(\tilde{\nu}_{\text{s}}^{\Delta}) = K \cdot (\tilde{\nu}_0 - \tilde{\nu})^3 \cdot [n(\tilde{\nu}) + 1] \cdot \left[\frac{E_{\text{loc}}^{\text{d}}(\tilde{\nu}_0 - \tilde{\nu})}{E_0(\tilde{\nu}_0 - \tilde{\nu})} \right]^2 \cdot \left[\frac{E_{\text{loc}}^{\text{d}}(\tilde{\nu}_0)}{E_0(\tilde{\nu}_0)} \right]^2 \cdot g^{\text{d}} \cdot \chi_{\text{vRS}}''(\tilde{\nu}) \quad (4)$$

for Stokes branch. Similarly, eSERS can be described as:

$$I_{\text{eSERS}}(\tilde{\nu}_{\text{as}}^{\Delta}) = K \cdot (\tilde{\nu}_0 + \tilde{\nu})^3 \cdot [n(\tilde{\nu}) + 1] \cdot \left[\frac{E_{\text{loc}}^{\text{m}}(\tilde{\nu}_0 + \tilde{\nu})}{E_0(\tilde{\nu}_0 + \tilde{\nu})} \right]^2 \cdot \left[\frac{E_{\text{loc}}^{\text{m}}(\tilde{\nu}_0)}{E_0(\tilde{\nu}_0)} \right]^2 \cdot g^{\text{m}} \cdot \chi_{\text{eRS}}''(\tilde{\nu}) \quad (5)$$

for anti-Stokes branch and

$$I_{\text{eSERS}}(\tilde{\nu}_{\text{s}}^{\Delta}) = K \cdot (\tilde{\nu}_0 - \tilde{\nu})^3 \cdot [n(\tilde{\nu}) + 1] \cdot \left[\frac{E_{\text{loc}}^{\text{m}}(\tilde{\nu}_0 - \tilde{\nu})}{E_0(\tilde{\nu}_0 - \tilde{\nu})} \right]^2 \cdot \left[\frac{E_{\text{loc}}^{\text{m}}(\tilde{\nu}_0)}{E_0(\tilde{\nu}_0)} \right]^2 \cdot g^{\text{m}} \cdot \chi_{\text{eRS}}''(\tilde{\nu}) \quad (6)$$

for Stokes branch. Here, E_0 denotes the far-field, and $E_{\text{loc}}^{\text{d}}$ and $E_{\text{loc}}^{\text{m}}$ describe the local fields in the dielectric phase and in the metal phase, respectively; the local field distribution is asymmetric across the meta/dielectric interface. g^{d} and g^{m} denote the coupling efficiencies of Raman transitions to the plasmonic cavity in the dielectric phase and metal phase, respectively; g^{d} explains the surface selection rules because the coupling efficiency is affected by the orientation and the position of molecular dipoles in a cavity. On the other hand, g^{m} would be less sensitive to $\tilde{\nu}_m$ because free electrons are the source of the signals. From Eqs. (1) and (5) or (2) and (6), one can obtain the radiative Purcell factor

for eSERS, $\left[\frac{E_{\text{loc}}^{\text{m}}(\tilde{\nu}_0 \pm \tilde{\nu})}{E_0(\tilde{\nu}_0 \pm \tilde{\nu})} \right]^2$, as follows:

$$I_{eSERS}/I_{eRS} = \left[\frac{E_{loc}^m(\tilde{\nu}_0 \pm \tilde{\nu})}{E_0(\tilde{\nu}_0 \pm \tilde{\nu})} \right]_2^2 \cdot \left[\frac{E_{loc}^m(\tilde{\nu}_0)}{E_0(\tilde{\nu}_0)} \right]_2^2 \cdot g^m \propto \left[\frac{E_{loc}^m(\tilde{\nu}_0 \pm \tilde{\nu})}{E_0(\tilde{\nu}_0 \pm \tilde{\nu})} \right]_2^2. \quad (7)$$

Now, one can expect that the ratio of the enhancement factor for vSERS, EF_{vSERS} , to that for eSERS, EF_{eSERS} , is nearly constant: $EF_{vSERS}/EF_{eSERS} \sim C$ when the Raman frequency shift $\tilde{\nu}$ is relatively small.

Then, we obtain:

$$\begin{aligned} I_{SERS}(\tilde{\nu}_{as}^\Delta) &= I_{eSERS}(\tilde{\nu}_{as}^\Delta) + I_{vSERS}(\tilde{\nu}_{as}^\Delta) \\ &= K \cdot (\tilde{\nu}_0 + \tilde{\nu})^3 \cdot [n(\tilde{\nu})] \cdot I_{eSERS}/I_{eRS} \cdot (\chi_{eRS}''(\tilde{\nu}) + C \cdot g^d \cdot \chi_{vRS}''(\tilde{\nu})) \\ &= K \cdot (\tilde{\nu}_0 + \tilde{\nu})^3 \cdot [n(\tilde{\nu})] \cdot I_{eSERS}/I_{eRS} \cdot \chi_{SERS}''(\tilde{\nu}) \end{aligned} \quad (8)$$

for anti-Stokes branch and

$$\begin{aligned} I_{SERS}(\tilde{\nu}_s^\Delta) &= I_{eSERS}(\tilde{\nu}_s^\Delta) + I_{vSERS}(\tilde{\nu}_s^\Delta) \\ &= K \cdot (\tilde{\nu}_0 - \tilde{\nu})^3 \cdot [n(\tilde{\nu}) + 1] \cdot I_{eSERS}/I_{eRS} \cdot (\chi_{eRS}''(\tilde{\nu}) + C \cdot g^d \cdot \chi_{vRS}''(\tilde{\nu})) \\ &= K \cdot (\tilde{\nu}_0 - \tilde{\nu})^3 \cdot [n(\tilde{\nu}) + 1] \cdot I_{eSERS}/I_{eRS} \cdot \chi_{SERS}''(\tilde{\nu}) \end{aligned} \quad (9)$$

for Stokes branch, where $\chi_{SERS}''(\tilde{\nu}) \equiv \chi_{eRS}''(\tilde{\nu}) + C \cdot g^d \cdot \chi_{vRS}''(\tilde{\nu}) = \chi_{eSERS}''(\tilde{\nu}) + \chi_{vSERS}''(\tilde{\nu})$. When the radiative Purcell factor, I_{eSERS}/I_{eRS} in Eq. 7, is obtained experimentally, a measured SERS spectrum can be converted to the DOS format, $\chi_{SERS}''(\tilde{\nu})$, by reducing the Purcell factor as well as the frequency factor and the BE thermal factor. The reduced spectrum, χ_{SERS}'' , consists of χ_{eSERS}'' and χ_{vSERS}'' , in which the former is normalized by χ_{eRS}'' and the latter expresses χ_{vRS}'' modified by the surface selection rules for SERS.

In the meantime, χ_{eRS}'' is proportional to the surface charge density of metal, n_s .³⁴ Although the

radiative Purcell factor, $\left[\frac{E_{loc}^m(\tilde{\nu}_0 - \tilde{\nu})}{E_0(\tilde{\nu}_0 - \tilde{\nu})} \right]_2^2$, also depends on n_s , the electrochemical potential dependence of the plasmon resonance property is relatively small. According to Eq. (6), therefore, the potential dependence of I_{eSERS} can be written as²⁵

$$\Delta I_{eSERS}(\tilde{\nu}_s^\Delta) \propto [n(\tilde{\nu}) + 1] \cdot \left[\frac{E_{loc}^m(\tilde{\nu}_0 - \tilde{\nu})}{E_0(\tilde{\nu}_0 - \tilde{\nu})} \right]_2^2 \cdot \Delta n_s. \quad (10)$$

This would be valid as long as Δn_s is small enough. Therefore, I_{eSERS} can be considered as a quasi-quantitative indicator of EDL charging in the absence of chemisorption.

2. eSERS spectrum of Au substrate

Fig. S1 shows SERS spectrum of the SERS-active Au surface measured under Ar-filled inert atmospheric condition, showing that the background continuum is not caused by fluorescence from [BMI]PF₆. A small feature in the THz range is ascribed to additional electronic Raman scattering induced by the relaxation of the momentum conservation due to surface roughness.²⁹

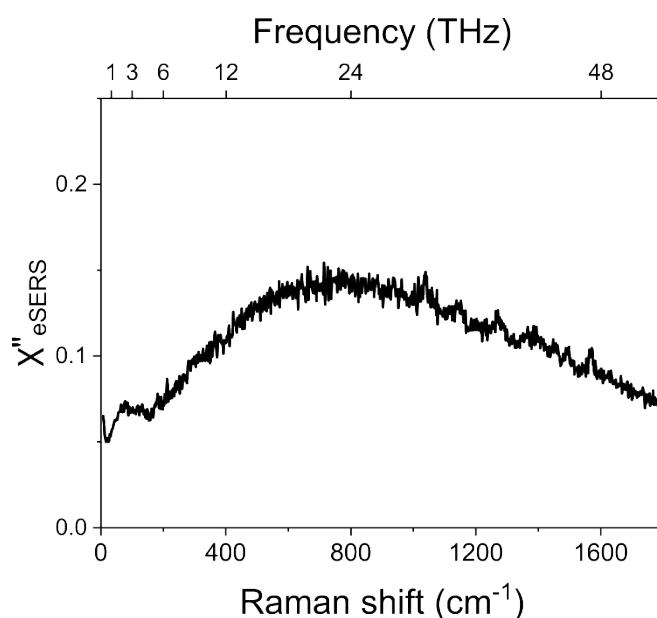


Fig. S1. SERS spectrum of SERS-active Au substrate in the reduced DOS format, measured under Ar-filled inert atmospheric condition in the absence of [BMI]PF₆.

3. Electrochemical SERS behaviours of [BMI]PF₆ on Au electrode

Fig. S2 shows 2D contour plots of electrochemical SERS spectra of [BMI]PF₆ on Au electrode under a potential cycle between 0.0 and -1.6 V within the electrochemical window. The $\nu_{\text{Au-PF}_6^-}$ at 741 cm^{-1} , BMI-related peaks in the range between $1200 - 1600 \text{ cm}^{-1}$, and $\nu_{\text{H}\cdots\text{F}}$ in the low-frequency range clearly show hysteresis behaviour in their potential-induced intensity variations. When the

applied potential approaches to the cathodic limit of the window, the hysteresis behaviour in SERS spectra variations becomes more significant as shown in Fig. S3. Fig. S4 compares characteristic features of the potential-induced spectral variations.

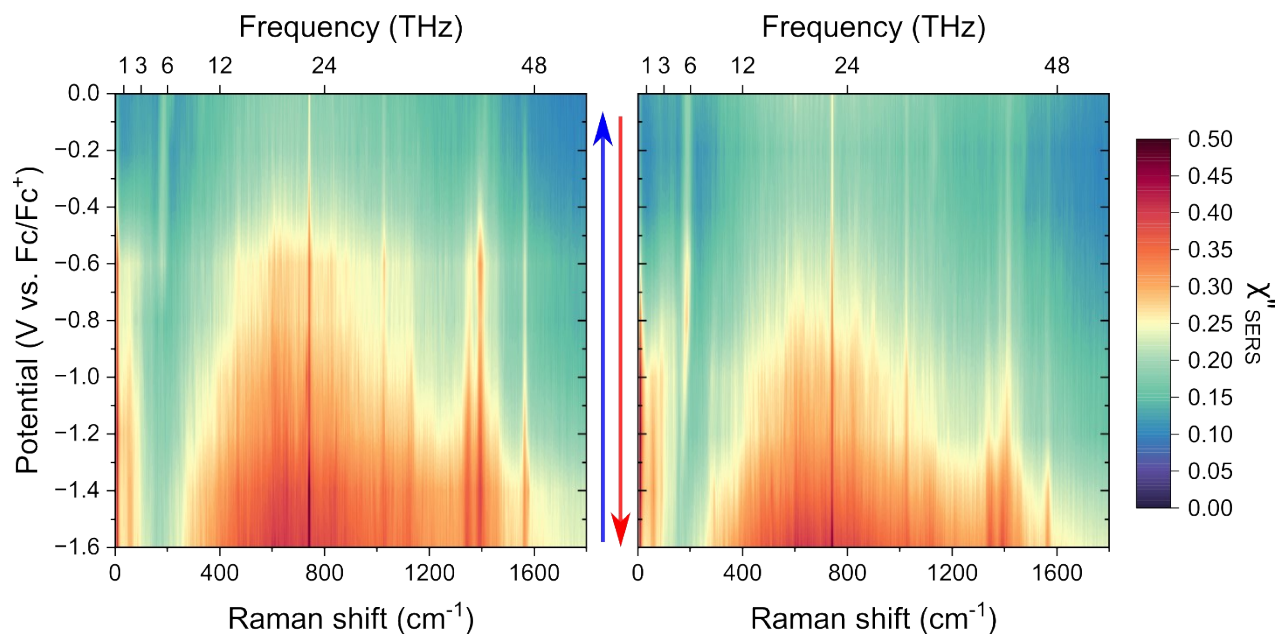


Fig. S2. 2D contour plots of electrochemical SERS spectra of [BMI]PF₆ on a SERS-active Au electrode in the reduced DOS format, measured under negative- and positive-going potential scans within the electrochemical window.

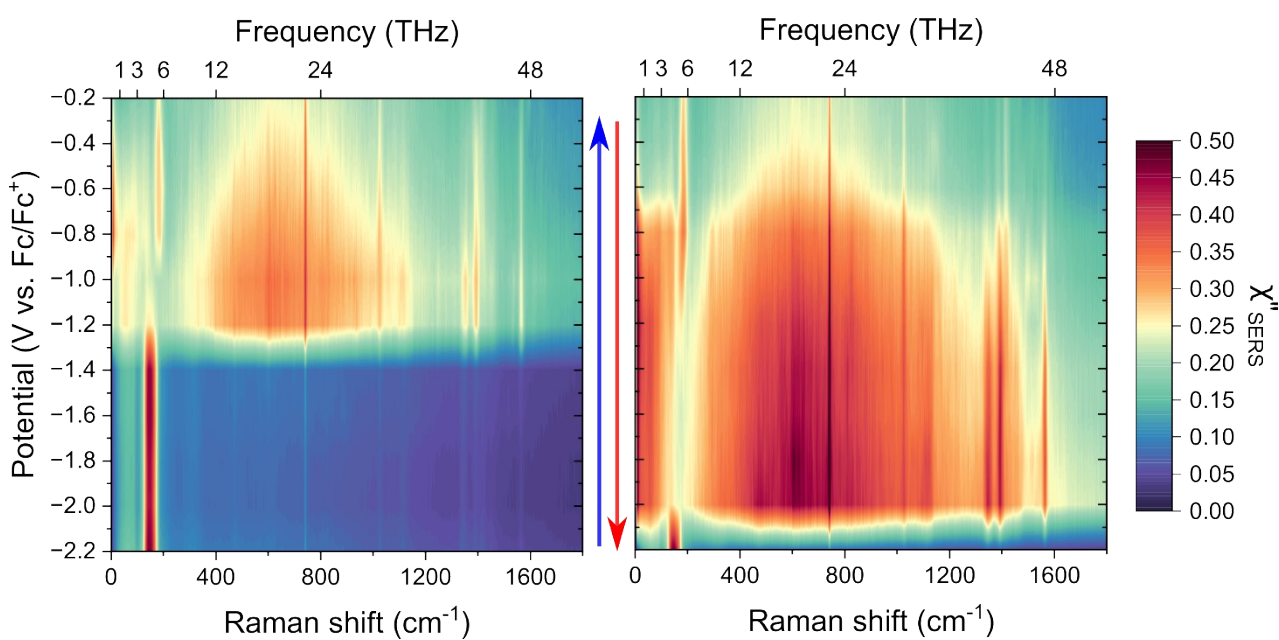


Fig. S3. 2D contour plots of electrochemical SERS spectra of [BMI]PF₆ on a SERS-active Au electrode in the reduced DOS format, measured under negative- and positive-going potential scans including the potential range where reductive deprotonation of [BMI]-cations occurs.

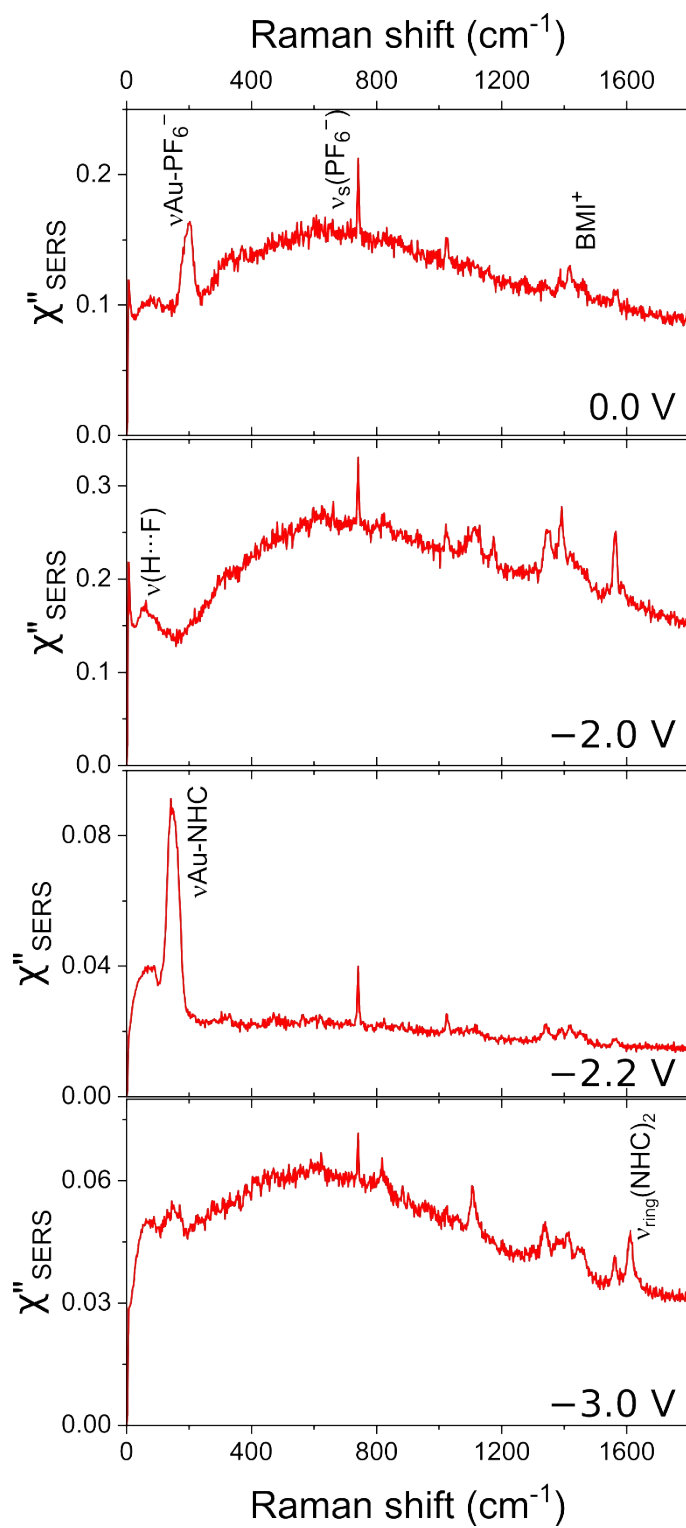


Fig. S4. A series of some selected SERS spectra of [BMI]PF₆ on Au surface taken under the negative-going potential scan.

4. DFT calculated Raman spectra

Vibrational calculations were carried out using the density functional theory (DFT) at the M06 level of theory with the def2-SVPD basis set, which were performed with the Gaussian09 ver.9.0 program. Fig. S5 shows the calculated Raman spectra for PF₆⁻-anion and PF₆⁻-Au₄. Fig. S6 shows the calculated results for BMI-cation, reductively deprotonated BMI (NHC), NHC-Au₄, and dimeric NHC.

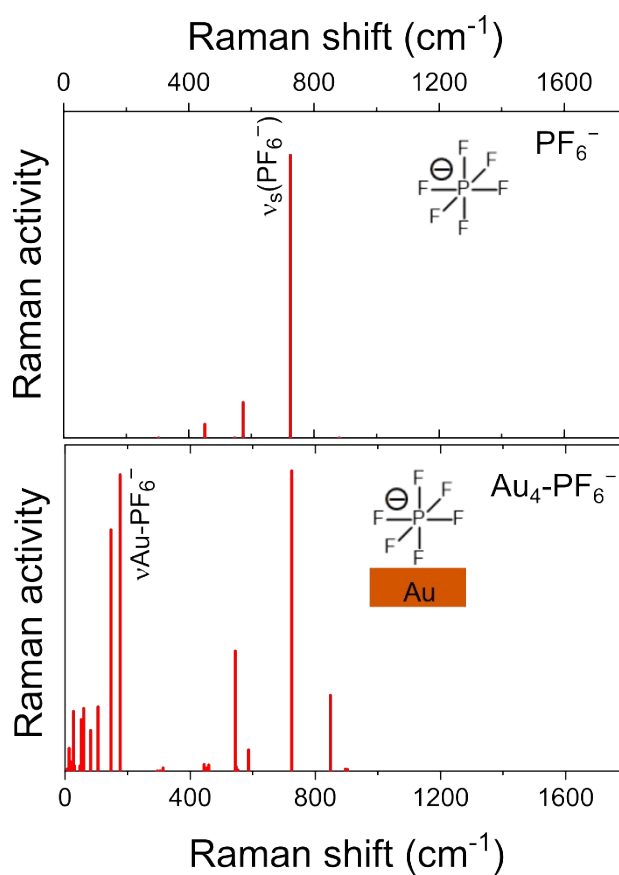


Fig. S5. DFT calculation results of Raman spectra for PF₆⁻-anion and PF₆⁻-Au₄.

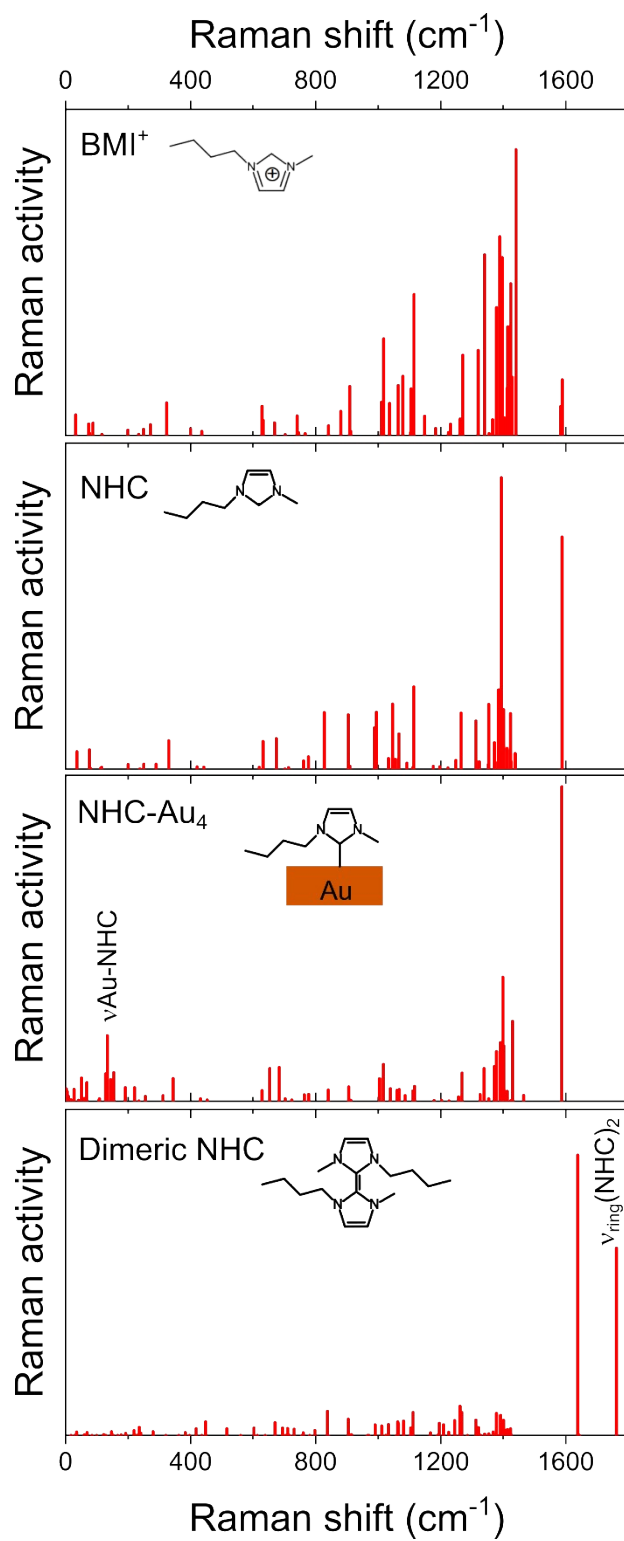


Fig. S6. DFT calculation results of Raman spectra for BMI-cation, NHC, NHC-Au₄, and dimeric NHC.